NJC

Accepted Manuscript

This is an *Accepted Manuscript*, which has been through the Royal Society of Chemistry peer review process and has been accepted for publication.

Accepted Manuscripts are published online shortly after acceptance, before technical editing, formatting and proof reading. Using this free service, authors can make their results available to the community, in citable form, before we publish the edited article. We will replace this *Accepted Manuscript* with the edited and formatted *Advance Article* as soon as it is available.

You can find more information about *Accepted Manuscripts* in the Information for Authors.

Please note that technical editing may introduce minor changes to the text and/or graphics, which may alter content. The journal's standard Terms & Conditions and the Ethical guidelines still apply. In no event shall the Royal Society of Chemistry be held responsible for any errors or omissions in this *Accepted Manuscript* or any consequences arising from the use of any information it contains.

ROYAL SOCIETY OF CHEMISTRY

www.rsc.org/njc

Journal Name

ARTICLE

Nitrite ion sensing properties of $ZnTiO_3$-TiO_2 composite thin films deposited from zinc-titanium molecular complex

Received 00th January 20xx,
Accepted 00th January 20xx

DOI: 10.1039/x0xx00000x

www.rsc.org/

Muhammad Ali Ehsan,[a] Hamid Khaledi, [a] Alagarsamy Pandikumar,[b] Perumal Rameshkumar,[b] Nay Ming Huang,[b] Zainudin Arifin,[a] Muhammad Mazhar*[a]

A titanium based heterobimetallic molecular precursor, $[Zn_2Ti_4(\mu\text{-}O)_6(TFA)_8(THF)_6]\cdot THF$ (**1**) (where TFA = trifluoroacetato; THF = tetrahydrofuran), has been designed and scrutinised for its various physicochemical properties by melting point, microanalysis, Fourier transform infra-red spectroscopy, proton nuclear magnetic resonance spectroscopy, thermogravimetry and single crystal X-ray structural analysis. The $ZnTiO_3$-TiO_2 composite thin films were grown on fluorine doped tin oxide (FTO) coated conducting glass substrate at 550 °C from three different solutions of (**1**) viz. methanol, THF and acetonitrile, by the aerosol-assisted chemical vapour deposition technique. The phase identification, chemical composition and microstructure of the fabricated thin films that were probed by powder X-ray diffraction, Raman spectroscopy, energy dispersive X-ray analysis and scanning electron microscopy revealed the formation of a 1:1 ratio of $ZnTiO_3$: TiO_2 composite microspheres of diverse designs and textures depending on the type of deposition solvent used. The direct band gap energy of 3.1 eV was estimated from UV-visible spectrophotometry of the $ZnTiO_3$-TiO_2 film fabricated from methanol solution and the film electrode was further tested as an electrochemical sensor for the detection of nitrite ions.

1. Introduction

Titanium dioxide (TiO_2) and titania-based nanocomposites are of enormous interest because of their excellent stability, non-toxicity and low-cost and therefore have been widely used as commercial materials ranging from white painting materials,[1] beam splitters,[2] optical,[2] antireflection[2] and corrosion-protective coatings,[2] gas sensors,[3] solar cells,[4] electric and electrochromic devices [5] to biocompatible bone implants.[6] In addition, TiO_2 also finds applications in photoinduced hydrophilicity, being utilized for self-cleaning purposes, which allows for greater wetting of a surface as well as the formation of electron/hole pairs for dirt removal.[7-9] There are a number of conventional synthetic routes [10-15] available for the synthesis of pure $ZnTiO_3$ powders and thin films which often generate the TiO_2 phase as an impurity or secondary phase. However, we have erudited that the targeted synthesis of 1:1 ratio of $ZnTiO_3$:TiO_2 nanocomposite powders and thin films has not been extensively reported so far.[16, 17] Moreover many of the reported synthetic methods suffer from multiple drawbacks. For example, solid state methods involve extensive heating and grinding steps, dissipate rigorous energy and time and do not generate well defined products. Batch hydrothermal methods are prone to batch to batch variations and do not offer similar product quality when scaled-up; magnetron sputtering methods are difficult to scale-up and can only be carried out on small-sized substrates. In order to overcome these limitations, much attention has been paid for the development of alternative single-source molecular precursors during the last decade.

The design and development of molecular precursor reagents for chemical vapour deposition (CVD) is a well-established route to create thin films with potential advantages such as high crystallinity, spatially oriented nanostructure, excellent control over homogeneity, stoichiometry and reproducibility of the final product at relatively lower temperatures. To date, few Zn-Ti molecular complexes such as $[Zn(H_2O)_5]_2[Ti(O_2)_2O(nta)_2]\cdot 7H_2O$,[18] $Cp_2Ti(OCH_2CH_2OZnEt)_2$[19] and $Zn_2Ti_4(\mu_3\text{-}O)_2(\mu_2\text{-}O)_2(O\text{i}Pr)_2(\mu_2\text{-}OMc)_{10}$ [20] are known and none of these compounds has been employed as CVD precursors for the deposition Zn–Ti ceramic oxides.

Our step by step synthesis has resulted in numerous well defined titanium-based heterobimetallic complexes such as $[Mn_2Ti_4(TFA)_8(THF)_6(OH)_4(O)_2]\cdot 0.4THF$,[21] $[Fe_2Ti_4(\mu\text{-}O)_6(TFA)_8(THF)_6]$,[22] $[Co_2Ti(\mu_3\text{-}O)(TFA)_6(THF)_3]$,[23] $[Ni_2Ti_2(OEt)_2(\mu\text{-}OEt)_6(acac)_4]$,[24] $[Ti_4(dmae)_6(\mu OH)(\mu\text{-}O)_6Cu_6(benzoate)_9]$,[25]

[a] Department of Chemistry, Faculty of Science, University of Malaya, Lembah Pantai, 50603 Kuala Lumpur, Malaysia; E-mail: maligau@ymail.com ; *mazhar42pk@yahoo.com; hamid.khaledi@gmail.com; zainudin@um.edu.my, . Tel: +60(03)79674269..
[b] Low Dimensional Materials Research Centre, Department of Physics, Faculty of Science, University of Malaya, 50603 Kuala Lumpur, Malaysia; E-mail: huangnayming@gmail.com; pandikumarinbox@gmail.com; rameshkumar.mku@gmail.com Tel: +6012-2091008.Address

† CCDC 1026550 contains the supplementary crystallographic data for this paper. These data can be obtained free of charge from The Cambridge Crystallographic Data Centre *via* www.ccdc.cam.ac.uk/data_request/cif..
Electronic Supplementary Information (ESI) available: [Micro analysis results, H-NMR spectrum, IR spectrum, X-ray diffraction pattern, Energy dispersive X-ray spectra, electrochemical plots]. See DOI: 10.1039/b000000x/

$[Ti_4(dmae)_6(\mu\text{-}OH)(\mu\text{-}O)_6Cu_6(2\text{-methylbenzoate})_9]$[25], $[Ti_4(dmae)_6(\mu\text{-}OH)(\mu\text{-}O)_6Cu_6(OAc)_9H_2O]$[26], $[Cd_4Ti_4(dmae)_4(TFA)_8(OAc)_4O_6]$[27] and $[PbTi(\mu_2\text{-}O_2CCF_3)_4(THF)_3(\mu_3\text{-}O)]_2$[28]. The protraction of our previous synthetic strategy motivated us to bring Ti and Zn metals into one framework through an eminent bridging trifluoroacetato (CF_3COO^-) moiety to develop Zn–Ti bimetallic complex that proved a natural precursor for oxide materials. Current work detailing the synthesis and characterization of the heterobimetallic precursor $[Zn_2Ti_4(\mu\text{-}O)_6(TFA)_8(THF)_6]\cdot THF$ (**1**) (where TFA = trifluoroacetato, THF = tetrahydrofuran) and its disposal for the deposition of $ZnTiO_3$-TiO_2 composite films on fluorine-doped tin oxide (FTO) coated conducting glass substrates by aerosol assisted chemical vapour deposition (AACVD) at the relatively low temperature of 550 °C is reported here. Thin films prepared from methanol, THF and acetonitrile solutions of (**1**) were characterised by X-ray diffraction (XRD), Raman spectroscopy, scanning electron microscopy (SEM), energy dispersive X-ray (EDX) and ultraviolet visible (UV–Vis) spectroscopy to determine the extent of crystallinity, morphology, stoichiometry and optical band gap properties. Furthermore, the $ZnTiO_3$-TiO_2 composite thin film fabricated from methanol was used for the construction of electrochemical sensor for the detection of nitrite (NO_2^-) ions which is a well-known natural contaminant in drinking water that causes methemoglobinemia, or "blue baby" syndrom in humans.[29] The $ZnTiO_3$-TiO_2 composite thin film showed NO_2^- ion detection limits of 15.62 and 3.98 µM, as measured by linear sweep voltammetry (LSV) and amperometric i-t curve techniques respectively. Moreover, the present electrochemical sensor is sensitive and selective towards the detection of NO_2^- ions in the presence of other common interferents.

2. Experimental

2.1. Material and methods

All manipulations were carried out under an inert atmosphere of dry argon using Schlenk tubes fitted with vacuum line and hot plate arrangements. The solvent was rigorously dried over sodium benzophenoate and distilled immediately before use. Zinc (II) acetate ($Zn(CH_3COO)_2$), titanium (IV) isopropoxide ($Ti(OCH(CH_3)_2)_4$) and trifluoroacetic acids (CF_3COOH) were purchased from Aldrich Chemical Co. The reagents were used as received. The melting point was determined in a capillary tube using an electrothermal melting point apparatus; model MP.D Mitamura Riken Kogyo (Japan). The elemental analyses were performed using Leco CHNS 932. Fourier transform infra-red (FT-IR) spectrum was recorded on a single reflectance ATR instrument (4000–400 cm^{-1}, resolution 4 cm^{-1}). The proton nuclear magnetic resonance (^{1}H-NMR) spectrum was recorded by JEOL DELTA2 NMR Spectrometer at field strength of 400MHz using methanol-D as a solvent. The controlled thermal analysis was investigated using a Perkin Elmer TGA 4000 thermogravimetric analyzer with a computer interface. The thermal measurements were carried out in a ceramic crucible under an atmosphere of flowing nitrogen (50 mL min^{-1}) with a heating rate of 10 °C min^{-1}.

2.2. Synthesis of $[Zn_2Ti_4(\mu\text{-}O)_6(TFA)_8(THF)_6]\cdot THF$ (1)

Precursor (**1**) was prepared by mixing stoichiometric amounts of 0.50 g (2.72 mmol) of $Zn(CH_3COO)_2$ and 1.61 mL (5.45 mmol) of $Ti(OCH(CH_3)_2)_4$ followed by the addition of 0.83 mL (10.90 mmol) of CF_3COOH in 25 mL of THF in a 50mL Schlenk tube. The reaction mixture was stirred for 4h and solvent was evacuated under vacuum to obtain a white powder which was redissolved in THF. The resulting transparent solution was cannula-filtered and placed at room temperature for 3 days to obtain the yellow block shape crystals of precursor (**1**) in 70% yield.

Mp: 225 °C (decomposition). Elemental analysis, (Found: C, 27.96; H, 2.87. $C_{44}H_{56}F_{24}O_{29}Zn_2Ti_4$ requires C, 28.90; H, 3.06 %). IR: ν_{max}/cm^{-1} 1715s, 1678s, 1526w, 1470s, 1196s, 1145s, 1039w, 1024s, 891s, 846s, 793s, 721s, 682w, 656w, 617s, 520s. ^{1}H NMR δ = 3.70 ppm [m, 2H, C*H*2O] and δ = 1.80 ppm [m, 2H, C*H*2]. TGA: 40-95 °C (5.10% wt. loss); 96-178 °C (13.0% wt. loss); 180-260 °C (30.81% wt. loss), 260-500 °C (24.39% wt. loss) (Residual mass of 26.70%); (Cal. for $ZnTiO_3/TiO_2$ 26.38%).

2.3. Single-crystal X-ray crystallography

The diffraction data for precursor (**1**) were collected on a Bruker SMART Apex II CCD area-detector diffractometer (graphite-monochromatized Mo-*Kα* radiation, λ = 0.71073 Å) at 133(2) K. The orientation matrix, unit cell refinement and data reduction were all handled by the Apex2 software (SAINT integration, SADABS multi-scan absorption correction) [30]. The structure was solved using direct methods in the program SHELXS-97 [31] and was refined by the full matrix least-squares method on F^2 with SHELXL-2014/7. All the non-hydrogen atoms were refined anisotropically. All the hydrogen atoms were placed at calculated positions and were treated as riding on their parent atoms. The structure exhibits a whole molecule disorder with the two components being related by a pseudo-inversion centre. The occupancy of the main component refined to 0.675(2). The structure was also refined as a racemic twin with the twin parameter of 0.42(3). Drawing of the molecule was produced with XSEED.[32]

2.4. AACVD studies

In continuation of an earlier work[21-28] on an in-house designed AACVD assembly, $ZnTiO_3$-TiO_2 composite thin films were deposited on commercially available FTO coated conducting glass substrates. Before carrying out the deposition, the FTO glass substrates were cleaned with distilled water, acetone and ethyl alcohol, then placed inside a reactor tube and furnace (CARBOLITE, Model No. 10/25/130) (6"L × 1"D) and were heated up to a deposition temperature (550 °C) for 10 min. Deposition experiments were conducted using 20 mL of 0.1 M solution of precursor (**1**) in three different solvents viz. methanol, THF and acetonitrile. In a typical deposition experiment, a precursor solution was taken in a 50 mL round

bottom flask which was immersed in water bath above the piezoelectric modulator of an ultrasonic humidifier (Model No. Cool Mist-plus serial No. ADV-CMP-85956). Air at a flow rate of 100 mL min^{-1} was used as the carrier gas and the flow rate was controlled by an L1X linear flow meter. The generated aerosol droplets were then transferred into the hot wall zone of the reactor by the carrier gas. Both the solvent and the precursor were evaporated and the precursor vapour reached the heated substrate surface where thermally induced reactions and subsequent film deposition took place.

2.5. Thin film analysis

The XRD patterns of thin films were recorded on a PANanalytical, X'Pert HighScore diffractometer with primary monochromatic high intensity Cu-K_α (λ = 1.54184 Å) radiation over Bragg angles ranging from 15 to 90° in a step size of 0.026° and the operating voltage and current were maintained at 30 kV and 40 mA respectively. Raman spectroscopic measurements were carried out on a Renishaw InVia Raman microscope and excitation was performed using the 514 nm line of Argon laser with a 0.01 mW output power. The surface morphology and chemical composition of thin films were analysed by field-emission scanning electron microscope (Hitachi FESEM SU 8000) equipped with EDX spectrometer (INCA Energy 200, Oxford Inst.) operated at an accelerating voltage of 20 kV and a working distance of 9.2 mm. The optical absorbance of thin films deposited from methanol solution of (**1**) having thickness of 300 nm (profilometer KLA Tencore P-6 surface profiler) was recorded on a Lambda 35 Perkin-Elmer UV–Vis spectrophotometer in the wavelength range of 300–900 nm.

2.6. Electrochemical sensor studies

All the electrochemical experiments were performed in a single compartment three–electrode cell at room temperature using a PAR-VersaSTAT-3 Electrochemical workstation. The $ZnTiO_3$-TiO_2 composite thin film and a platinum wire were used as working and counter electrodes, respectively. Silver/silver chloride (Ag/AgCl) electrode was used as a reference electrode. A 0.1 M phosphate buffer solution (PBS) (pH 7.2) was used as a supporting electrolyte for the electrochemical experiments and all the potentials are quoted against Ag/AgCl reference electrode unless otherwise mentioned.

3. Results and discussion

3.1. Preparation and characterization of precursor (1)

The hexanuclear precursor $[Zn_2Ti_4(\mu\text{-}O)_6(TFA)_8(THF)_6]\cdot THF$ (**1**) was prepared by a chemical reaction of diacetatozinc(II) with tetrakisisopropoxytitanium(IV) in the presence of trifluoroacetic acid in dry THF. The reaction proceeds with the complete replacement of isopropoxo and acetato ligands attached to titanium and zinc centres respectively by the more strongly bonding trifluoroacetato ligands. Precursor (**1**) that was prepared in good yield has a zinc to titanium ratio of 1:2, is stable in air and shows high solubility in common organic solvents such as methanol, chloroform, acetonitrile and tetrahydrofuran.

The stoichiometry of the precursor (**1**) has been formulated on the basis of elemental analysis, FT-IR, ^{1}H-NMR and single crystal X-ray analyses as summarized in Experimental Section. The FT-IR spectrum of precursor (**1**) shows the presence of characteristic vibrations of functional groups attached to the zinc and titanium atoms. The typical symmetric and asymmetric ν(C=O) absorptions of trifluoroacetato ligand arose at 1674 and 1466 cm^{-1} respectively. The difference in value of 208 cm^{-1} between symmetric and asymmetric ν(C=O) absorption bands reveals the bidentate behaviour of the carboxylato group of trifluoroacetato ligand that is bonded to different metal centres.[21-23] Similarly, the peak at 1195 cm^{-1} confirms the presence of C–F bonds in precursor (**1**).[21-23] ^{1}H-NMR spectrum showed two signals at 1.80 ppm [m, 2H, CH_2] and 3.70 ppm [m, 2H, CH_2O] respectively due to the presence of THF molecules.

3.2. Molecular structure of precursor $[Zn_2Ti_4(\mu\text{-}O)_6(TFA)_8(THF)_6]\cdot THF$ (1)

The single crystal X-ray structure of precursor (**1**) is shown in Fig. 1. The crystal data and structure refinement details are summarized in Table 1 while Table 2 lists the selected bond lengths and angles for the crystal structure (**1**).

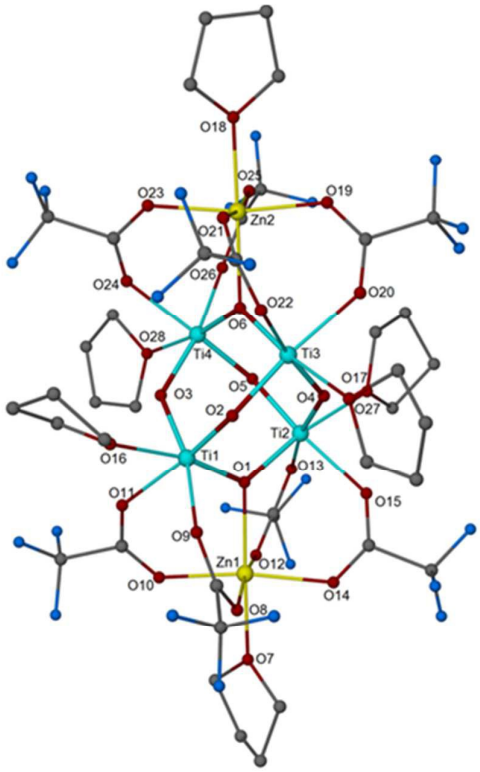

Fig. 1. Crystal structure of precursor $[Zn_2Ti_4(\mu\text{-}O)_6(TFA)_8(THF)_6]\cdot THF$ (**1**). The minor component of disorder, hydrogen atoms, and the solvate THF molecule are not shown.

The molecular structure of (**1**) resembles that of the analogous Fe-Ti heterometallic complex.[22] The precursor molecule has a non-crystallographic D_2 point symmetry. It contains four Ti^{4+} and two Zn^{2+} metal centers all being octahedrally coordinated by O atoms. The four Ti atoms are located at the corners of a tetrahedron and are bridged by six oxides into an adamantane-like Ti_4O_6 cage. Two of the cage oxide atoms (O1, O6) are of the μ_3-type and each bridges two Ti atoms to a Zn atom. For the triply-bridged O atoms, the Ti-O distances (ave. 1.890 Å) are considerably shorter than the Zn-O distances (ave. 2.184 Å). Four cage oxygen atoms (O2, O3, O4, O5) are μ_2 and only bridge two titanium atoms with distances ranging from 1.781 – 1.841 Å. The Ti-Ti distances are in the narrow range of 3.331-3.350 Å (Table 1). These parameters compare well with those found in similar Ti_4O_6 structures. [25, 26, 33] The octahedral environment around the metals is completed by two bridging trifluoroacetato's (TFA) ligand and one THF in the case of Ti, and four bridging TFA's groups and one THF in the case of Zn.

Table 1: Crystal data and refinement parameters for $[Zn_2Ti_4(\mu\text{-}O)_6(TFA)_8(THF)_6]\cdot THF$ (**1**)

Empirical formula	$C_{44}H_{56}F_{24}O_{29}Ti_4Zn_2$
Formula weight	1827.22
Crystal system	orthorhombic
Space group	$Pca2_1$
a	19.2529(2) Å
b	20.8320(3) Å
c	17.2971(3) Å
Volume	6937.46(17) Å^3
Z, density (calculated)	4, 1.749 mg /m^3
Reflections collected	63498
Unique reflections	15266 (R_{int} = 0.0301)
Observed reflections [($I > 2\sigma(I)$]	12687
Final *R* indices [($I > 2\sigma(I)$]	R_1 = 0.0702, wR_2 = 0.1943
CCDC No.	1026550

Table 2: Selected bond distances and bond angles for $[Zn_2Ti_4(\mu\text{-}O)_6(TFA)_8(THF)_6]\cdot THF$ (**1**)

Bond Distances (Å)			
Zn1-O8	2.036(7)	Zn2-O21	2.026(8)
Zn1-O10	2.045(8)	Zn2-O25	2.028(8)
Zn1-O12	2.050(8)	Zn2-O19	2.043(9)
Zn1-O14	2.058(8)	Zn2-O23	2.047(8)
Zn1-O7	2.145(6)	Zn2-O18	2.129(7)
Zn1-O1	2.180(6)	Zn2-O6	2.187(6)
Ti1-O1	1.870(6)	Ti3-O22	2.085(10)
Ti1-O2	1.813(7)	Ti3-O27	2.148(10)
Ti1-O3	1.818(7)	Ti4-O3	1.825(7)
Ti1-O9	2.074(10)	Ti4-O5	1.809(6)
Ti1-O11	2.085(10)	Ti4-O6	1.898(7)
Ti1-O16	2.127(10)	Ti4-O24	2.093(8)
Ti2-O1	1.921(7)	Ti4-O26	2.125(10)
Ti2-O4	1.833(7)	Ti4-O28	2.128(11)
Ti2-O5	1.790(7)	Ti1-Ti3	3.331(3)
Ti2-O13	2.120(10)	Ti1-Ti2	3.343(3)
Ti2-O15	2.103(9)	Ti1-Ti4	3.345(3)
Ti2-O15	2.103(9)	Ti2-Ti4	3.330(3)
Ti2-O15	2.103(9)	Ti2-Ti3	3.350(3)
Ti3-O4	1.781(7)	Ti3-Ti4	3.349(3)
Ti3-O4	1.781(7)	Ti3-O22	2.085(10)
Bond Angles [°]			
O8-Zn1-O10	94.0(4)	O2-Ti1-O3	95.9(3)
O8-Zn1-O12	168.8(3)	O2-Ti1-O1	99.7(3)
O10-Zn1-O12	87.0(5)	O3-Ti1-O1	99.0(3)
O8-Zn1-O14	86.9(4)	O2-Ti1-O9	88.5(4)
O10-Zn1-O14	171.2(3)	O3-Ti1-O9	166.4(4)
O1-Zn1-O14	90.4(5)	O1-Ti1-O9	92.9(3)
O8-Zn1-O7	85.8(3)	O2-Ti1-O11	166.8(4)
O8-Zn1-O7	85.8(3)	O3-Ti1-O11	87.2(4)
O12-Zn1-O7	83.2(3)	O1-Ti1-O11	92.4(3)
O14-Zn1-O7	85.4(3)	O4-Ti2-O13	167.7(3)
O8-Zn1-O1	95.7(3)	O1-Ti2-O13	94.8(3)
O10-Zn1-O1	95.0(3)	O15-Ti2-O13	84.1(5)
O12-Zn1-O1	95.2(3)	O5-Ti2-O17	89.6(4)
O14-Zn1-O1	93.6(3)	O4-Ti2-O17	89.4(4)
O7-Zn1-O1	178.2(3)	O4-Ti2-O13	167.7(3)
O21-Zn2-O25	170.2(3)	O1-Ti2-O13	94.8(3)
O21-Zn2-O19	91.1(5)	O1-Ti2-O17	170.6(4)
O25-Zn2-O19	88.4(5)	O15-Ti2-O17	80.0(4)
O21-Zn2-O23	87.6(5)	O13-Ti2-O17	79.0(4)
O25-Zn2-O23	91.3(5)	O4-Ti3-O2	94.3(3)
O19-Zn2-O23	170.5(3)	O4-Ti3-O6	98.4(3)
O21-Zn2-O18	84.0(3)	O2-Ti3-O6	98.4(3)
O25-Zn2-O18	86.2(3)	O4-Ti3-O22	167.1(3)
O19-Zn2-O18	85.7(3)	O2-Ti3-O22	89.0(4)
O23-Zn2-O18	84.8(3)	O6-Ti3-O22	93.5(3)

3.3. Thermal (TG/DTG) analysis of complex (1)

The thermal behaviour of the complex (**1**) has been investigated by simultaneous thermogravimetric (TG) and derivative thermogravimetric (DTG) analysis to monitor the step wise decomposition of the precursor compound and the formation of the target material that may undergo any phase change during analysis (Fig. 2). The optimum temperature suitable for the thermal decomposition of the precursor was

also investigated and implemented for the deposition of thin films.

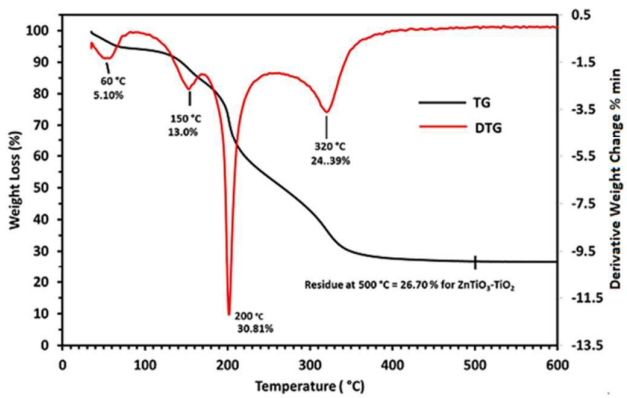

Fig. 2. TG/DTG curves showing complete thermal degradation of precursor (**1**) to give clean $ZnTiO_3$-TiO_2 composite oxide materials.

The DTG data reveal that complete thermal decomposition of precursor (**1**) proceeds in four distinct steps of maximum heat gain at 60, 150, 200 and 320 °C. The TG curve indicates that the initial pyrolysis phase of (**1**) occurs between 40–95 °C and represents a loss of 5.10 % of the sample that matches the loss of lattice THF molecule from the sample. The second stage of the degradation of (**1**) falls in the temperature range of 96–178 °C and experiences a weight loss of 13.00%. This loss in weight corresponds to the loss of three bonded THF molecules (ca.12.30%). The third and major breakdown phase lies in a temperature array of 180–260 °C, to eliminate the remaining three THF and two TFA groups and reflects a weight loss of 30.81 %. At this stage most of the core structure of the precursor has collapsed. The weight loss terminates at 500 °C by an amount of stable residue of 26.70% of the original mass of sample which accords well with the value 26.38% calculated for the expected 1:1 ratio of $ZnTiO_3$:TiO_2 composite oxide material.

Further sintering of the observed residue to the higher temperature of 600 °C did not experience any change in weight, suggesting that precursor (**1**) decomposes quantitatively to endow $ZnTiO_3$–TiO_2 as a stable final product.

3.4. Structural analysis

The initial thin film deposition experiment was conducted via AACVD using 0.1 M (20 mL) solution of precursor (**1**) in methanol on FTO substrate at a temperature of 550 ˚C in air atmosphere. The phase formation and degree of crystallinity of the obtained film were investigated by XRD technique and the result is displayed in Fig. S3a. It is worth noticing that peaks originating from crystalline tin oxide substrate overlap with the diffraction pattern of the deposit (Fig. S3b) and create problems in identifying the chemical nature and phase composition of the final product. Therefore, to avoid this ambiguity, films were also grown on plain glass substrate using different solutions of precursor (**1**) in methanol, THF and acetonitrile (ACN) under similar conditions and X-ray diffractograms are presented in Fig. 3. Apparently, all the XRD patterns of the films grown from three different solutions of (**1**) in methanol, THF and ACN look similar in terms of their peak positions and 2θ values and all the spectra are dominated by the diffraction peak located at 2θ = 32.80˚.

Further insights into the crystal structures and phase compositions of the deposits were gained by a careful inspection of each XRD pattern against standard Inorganic Crystal Structure Database (ICSD) which identifies the growth of ecandrewsite $ZnTiO_3$[36] (ICSD 98-002-2382) and a mixture of rutile[37] (98-003-9167) and anatase[38] (98-000-9852) phases in all cases (Fig S4a-c). In all films, the prepared $ZnTiO_3$ exists in a hexagonal crystal system with space group R-3 and produced characteristic peaks indicated by (*) at 2θ = 21.1, 23.9, 32.8, 35.3, 38.7, 40.5, 49.0, 63.4, 70.9, 76.9, 78.6, 87.5˚ as observed by their Miller indices (101), (012), (104), (110), (006), (113), (024), (030), (1010), (306), (4-31), and (226) respectively. The emergence of peaks at 2θ = 25.3 (011), 38.5 (112), 48.0 (020) and 62.7˚ (024) denoted by (+) are well indexed to tetragonal anatase TiO_2. Furthermore, the peaks marked by (#) at 2θ = 27.4 (110), 36.0 (011), 41.2 (111) and 44.0˚ (120) are attributed to tetragonal rutile TiO_2. The X-ray diffractograms also demonstrate overlapped peaks between $ZnTiO_3$ and anatase TiO_2 phases at 2θ values of 53.8, 62.0 and 75.0˚. A few common reflections originating from both $ZnTiO_3$ and rutile TiO_2 phases appear at 2θ values of 56.5, 63.9, 79.7 and 81.8˚. Moreover, diffraction peaks at 2θ values of 63.5, 68.8 and 87.2˚ are shared by all three crystalline $ZnTiO_3$, anatase TiO_2 and rutile TiO_2 phases present in the deposit. No possible crystalline impurities such as Zn_2TiO_4, $Zn_2Ti_3O_8$ and ZnO were detected from these XRD patterns.

The XRD qualitative phase analysis reveals that all the zinc titanate-titania composite films deposited from three different solvents have similar crystalline phases of hexagonal $ZnTiO_3$ and a mixture of anatase and rutile TiO_2. Subsequently the XRD semi-quantification analysis was applied on each X-ray diffractogram to measure the proportion of crystallinity of each phase in the crystalline composite product. The crystalline composition of $ZnTiO_3$-TiO_2 deposit obtained from methanol is poised at 54% $ZnTiO_3$ (*), 29% rutile TiO_2 (#) and 17% anatase TiO_2 (+), respectively (inset Fig. 3a). However the film deposited from THF contains the crystalline contents of 76% $ZnTiO_3$ (*), 12% rutile (#) and 12% anatase TiO_2 (+) (inset Fig. 3b). The percentage ratio of crystallinity in $ZnTiO_3$-TiO_2 deposited from ACN varies as follows: 85% $ZnTiO_3$ (*), 12% rutile (#) and 3% anatase TiO_2 (+) (inset Fig. 3c). It is worth stressing that the films obtained from three different solvents differ in terms of their percentage crystalline composition of the phases, however the overall phase composition of 1: 1 for $ZnTiO_3$: TiO_2 can be further confirmed from energy dispersive X-ray analysis.

The variations in crystalline composition of the films formed from different solvents suggest that solvents play a key role in dictating the crystalline phases of the films grown on the substrate surface by AACVD, and not just as a transport

medium. In aerosol deposition, solvents play an important role in the determination of the extent of a reaction. The precursor can react differently in various solvents in the gas phase which may lead to the formation of different intermediates and thus to different phases of the deposit. There have been similar reports whereby a variety of solvents have been used to alter the phase composition of titania using sol-gel approach, spray pyrolysis and AACVD. [39,40]

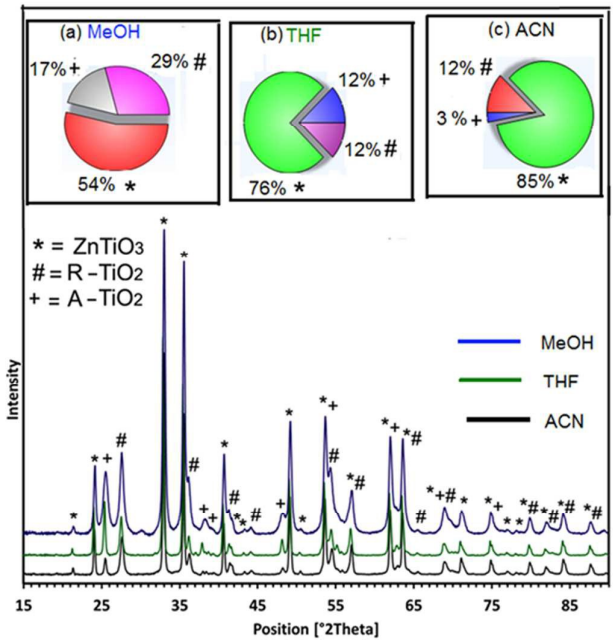

Fig. 3. X-ray diffractogram of the $ZnTiO_3$-TiO_2 composite thin film prepared from solutions of (**1**) in methanol (blue line), THF (green line), ACN (black line) on plain glass at 550 °C in air ambient; Inset shows the phase compositions of the $ZnTiO_3$-TiO_2 films from (**a**) methanol 54% $ZnTiO_3$(*), 29% rutile TiO_2(#), 17% anatase TiO_2(+); (**b**) THF 76% $ZnTiO_3$(*), 12% rutile TiO_2(#), 12% anatase TiO_2(+)and (**c**) ACN 85% $ZnTiO_3$(*), 12% rutile TiO_2(#), 3% anatase TiO_2 (+).

Recent literature implies that attempts to synthesize pure $ZnTiO_3$ generally require higher temperatures exceeding 700 °C and often produce TiO_2 and $Zn_2Ti_3O_8$ as impurity phases. Furthermore, it needs prolonged annealing at the higher temperature of 800 °C to enhance the crystallinity of the material.[10-15] It is also known that bulk $ZnTiO_3$ is stable up to 875 °C and higher annealing temperatures deteriorate $ZnTiO_3$ into Zn_2TiO_4 along with TiO_2 and ZnO phases.[41] The instability of $ZnTiO_3$ at higher temperatures is attributed to weaker metal–oxygen bonds as compared to those of the other compounds (Zn_2TiO_4, ZnO, and TiO_2) present in the ZnO–TiO_2 system. [36] A similar result has been demonstrated in the $ZnTiO_3$ thin films annealed at 900 °C.[42] Solid-state synthesis based on ball milling of ZnO and TiO_2 nanopowders at thermal annealing temperatures higher than 900 °C reveals a similar result.[43] The $ZnTiO_3$ precursor solution derived from a sol–gel technique shows that the high calcination temperature of 1000 °C results in the formation of a pure Zn_2TiO_4 phase.[44] On the other hand, in the present case, precursor (**1**) cleanly decomposes at the relatively low temperature of 550 °C to furnish a high crystalline 1:1 ratio composite of $ZnTiO_3$:TiO_2 product free from all other zinc titanate (Zn_2TiO_4 and $Zn_2Ti_3O_8$) phases.

The Raman spectrum shown in Fig. 4 indicates that the $ZnTiO_3$-TiO_2 composite oxide thin films on soda lime glass identifies as zinc titanate and titania phases as also supported from XRD analysis. The Raman scattering vibration modes detected at 264, 344, 462, and 711 cm^{-1}, are characteristic of hexagonal $ZnTiO_3$. The peaks located at 144, 391, 516 cm^{-1} correspond to tetragonal anatase TiO_2 phase while peaks at 230 and 622 cm^{-1} represent tetragonal rutile TiO_2 phase in the $ZnTiO_3$-TiO_2 composite film. The Raman spectroscopy results are in good agreement with our XRD patterns and also matched well with the previously reported Raman data for the $ZnTiO_3$-TiO_2 composite materials.[16,45]

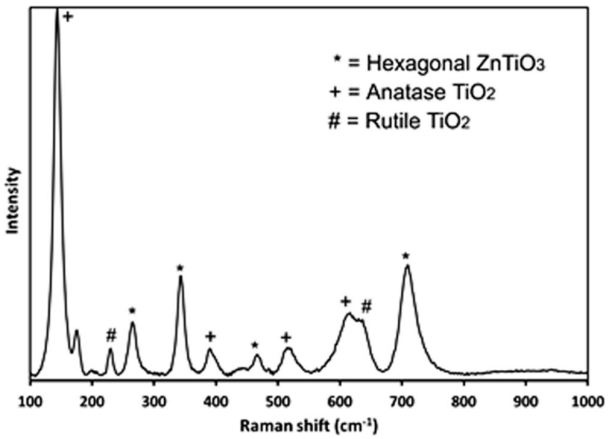

Fig. 4. Raman spectrum of $ZnTiO_3$-TiO_2 composite thin film deposited from methanol solution of (**1**) on plain glass substrate at 550 °C.

3.5. Microstructural properties

Recent work has established that the microstructure of the resulting thin film can be significantly modified by employing different deposition solvents in AACVD.[34,35] The solvent influences the deposition pathway by altering the aerosol droplet size and the thermodynamics of the processes taking place inside the deposition chamber. The physical properties of the solvents such as surface tension, density, viscosity and vapour pressure directly influence the aerosol droplet size and distribution at a constant frequency. As a consequence, the aerosol droplet size and distribution further influence the particle size and shape, morphology and texture of the deposited materials. The morphological variations in the films prepared from 0.1 M (20 mL) solution of precursor (**1**) in methanol, THF and ACN at 550 ˚C in air atmosphere were analysed by SEM.

Fig. 5 shows the surface and cross sectional SEM images of $ZnTiO_3$-TiO_2 composite film. Fig. 5(**a**) shows that the surface architecture of the film developed from methanol solution is composed of regularly connected microspheres of different sizes. Also depicted is the mixture of two different types of mesoporous microspheres in size range of 0.5-0.9µm. The

microsphere of one type contains tiny particles on the surface while the others are relatively bare. The low resolution surface SEM images (Fig. S5(**a1** and **a2**) reveal the that these mesoporous microspheres are homogenously distributed though out the film matrix.

The cross sectional view of $ZnTiO_3$-TiO_2 composite film of thickness 8.90 µm deposited from methanol solution displayed in Fig. 5(**b**) and Fig. S5(**b1**) show that small grains developed on the boundary layer of the FTO substrate.

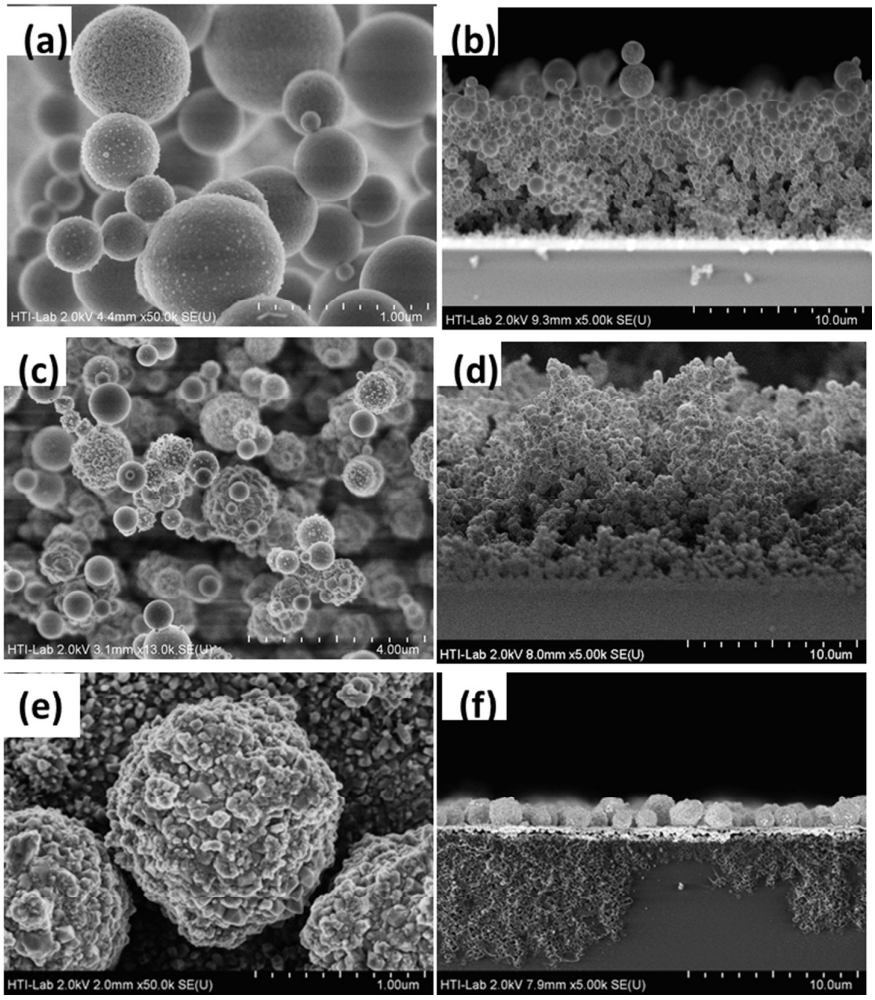

Fig. 5. (**a**), (**c**) and (**e**) show surface and (**b**), (**d**) and (**f**) indicate the cross sectional SEM images of $ZnTiO_3$-TiO_2 composite thin films deposited on FTO glass substrate at 550 °C from solution of precursor (**1**) in (**a, b**) methanol (**c, d**) THF and (**e, f**) acetonitrile, respectively.

Fig. 5(**c**) shows the surface morphology of $ZnTiO_3$-TiO_2 composite thin films grown from the THF solution of (**1**). The film consists of a set of interconnected spherical objects of different decoration which are grown in the vertical direction of the substrate plane. The enlarged views of the image depicts that the surface of one kind of spherical object of size 1.12 µm is fully covered with buds while the other type of microsphere of size 0.55 µm has a smooth and plain texture. The low resolution topographic images (Fig. S5(**c1** and **c2**) indicate that these heterogeneous spherical entities are evenly dispersed over the large area of the film.

Fig. 5(**d**) and Fig. S5(**d1**) designate the cross sectional view of the $ZnTiO_3$-TiO_2 composite film of thickness 11.4 µm deposited from THF solution.

Fig. 5**e** indicates the growth of spherical objects of size range of 0.9-2 µm of $ZnTiO_3$-TiO_2 composite thin films from ACN solution of (**1**). The texture of these objects appears rough and stony. The low resolution image further enables us to see the distribution of spheroid items over a wider area of the film (Fig. S5(e1 and e2)). The shape of the thin-film cross sections is shown in Fig. 5(**f**) and Fig. S5(**f1**) and a layer of spheroid

objects of thickness 1.67 µm can be clearly seen on the surface of the FTO substrate.

The deposited thin films are white in colour, uniform, robust, stable towards atmospheric conditions and adhere strongly on the FTO substrate as verified by the ''Scotch tape test''.

The stoichiometric compositions of all thin films determined by energy dispersive analysis (EDX) analysis (Fig. S6-8) performed at various random large areas revealed that the atomic ratio of Zn: Ti in the films is almost 1: 2 which is in accordance with the expected 1: 2 elemental ratio present in precursor (**1)** and also witness the homogeneity, uniformity and controlled stoichiometry of the films. The various peaks originating from the substrate elements (Sn, Si, Ca, Na, F) were not omitted from EDX spectra.

Since the films formed in methanol exhibit regularly connected features of porous microspheres as compared to the films formed from THF and acetonitrile, we therefore selected films deposited from methanol for nitrite ion sensing applications.

3.6. Optical properties

To investigate the light absorption properties of $ZnTiO_3$-TiO_2 films, the UV-vis absorption spectrum of the films prepared from a methanolic solution of (**1**) on FTO glass substrate was recorded for a wavelength range 330 to 850 nm as presented in Fig. 6.

The UV-vis spectrum indicates that the film shows a maximum absorbance in the UV region and a steep optical absorption starts from 400 nm. In order to evaluate the band gap of the films, Tauc's formula for direct band gap semiconductors is applied according to following equation (1):

$$(\alpha h\nu)^2 = A(h\nu - E_g) \ldots\ldots\ldots\ldots\ldots\ldots\ldots (1)$$

where α is absorption coefficient, A is a constant, $h\nu$ the photon energy. The corresponding Tauc's plot for $ZnTiO_3$-TiO_2 composite film of thickness 300 nm is shown in the inset of Fig. 6 giving a direct band gap energy, E_g, of 3.1 eV which accurately coincides with the recent work of other groups on crystalline composite $ZnTiO_3$-TiO_2 films.[16]

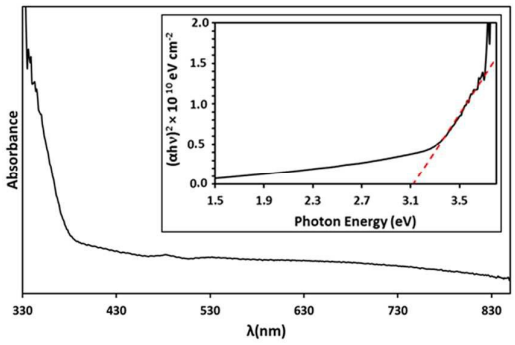

Fig. 6. UV–visible absorption spectrum of wavelength vs. absorption and inset Tauc's plot of photon energy vs. $(\alpha h\nu)^2$ of $ZnTiO_3$-TiO_2 thin films.

3.7. Electrochemical sensor application of $ZnTiO_3$-TiO_2 composite thin film for the detection of nitrite ion

The $ZnTiO_3$-TiO_2 composite electrode fabricated from methanol solution of (**1**) was used for the electrocatalysis and sensing of nitrite ions in 0.1 M phosphate buffer solution (PBS) (pH 7.2). The $ZnTiO_3$-TiO_2 composite electrode displayed a catalytic oxidation peak in the cyclic voltammogram for 1 mM of nitrite at +1.2 V (Fig. 7b) but did not show any voltammetric response in the absence of nitrite ions (Fig. 7a).

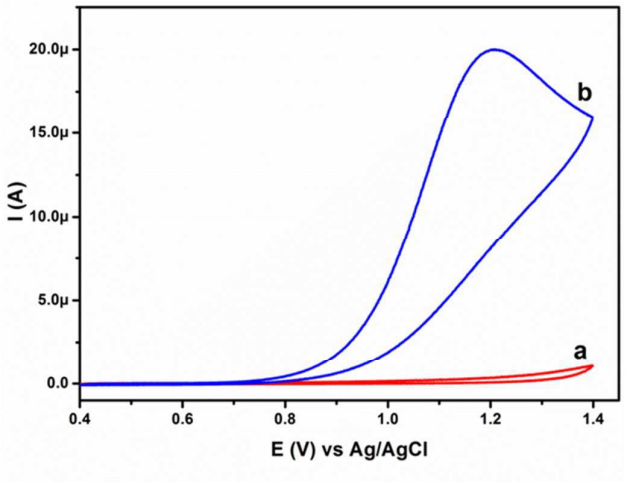

Fig. 7. Cyclic voltammograms obtained for $ZnTiO_3$-TiO_2 composite thin film in the (**a**) absence and (**b**) presence of 1 mM nitrite in 0.1 M PBS (pH 7.2) at a scan rate of 50 mV s^{-1}.

This unmistakably reveals that the composite oxide thin film facilitated the electron transfer kinetics for nitrite oxidation and during the electrochemical oxidation of nitrite, two electrons are transferred to form a nitrate ion as an oxidized product[46], according to equation (2):

$$NO^-_2 + H_2O \longrightarrow NO^-_3 + 2H^+ + 2e^- \qquad (2)$$

However, no characteristic oxidation peak current response was observed in the cyclic voltammogram for nitrite oxidation at the bare FTO electrode (Fig. S9).

The cyclic voltammogram of $ZnTiO_3$-TiO_2 film was recorded at different scan rates for 1 mM nitrite in 0.1 M PBS and are shown in Fig. 8A. The linear relationship between peak current and square root of scan rate (Fig. S10) concluded that the nitrite oxidation of the composite thin film is controlled by a diffusion process.[47]

The $ZnTiO_3$-TiO_2 composite film was employed as an electrochemical sensor for the detection of nitrite ions by using LSV and amperometric i-t curve techniques. The LSVs were recorded in 0.1 M PBS (pH 7.2) for the successive addition of 100 µM nitrite and the peak current increased linearly with respect to the concentration of nitrite (Fig. 8B).

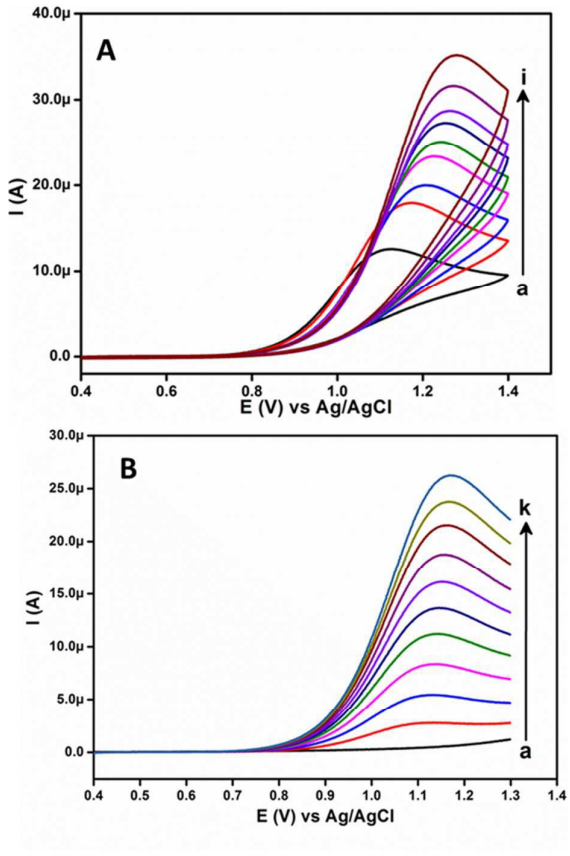

Fig. 8.(A) Cyclic voltammograms recorded for the $ZnTiO_3$-TiO_2 composite thin film in the presence of 1 mM nitrite in 0.1 M PBS (pH 7.2) at various scan rate of (**a-i**) 10-200 mV s^{-1}. (**B**) Linear sweep voltammograms obtained for the $ZnTiO_3$-TiO_2 composite thin film for each addition of 10 µM nitrite in 0.1 M PBS (pH 7.2) with a scan rate of 50 mV s^{-1}.

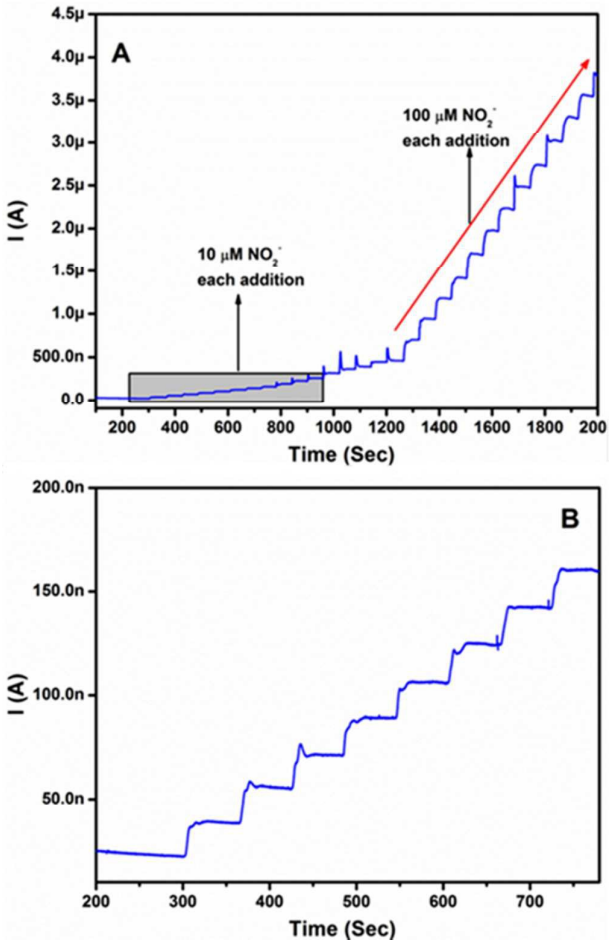

Fig. 9.(A) Amperometric i-t curve obtained for the $ZnTiO_3$-TiO_2 composite thin film for various additions of nitrite ion in 0.1 M PBS (pH 7.2) at a regular time interval of 60 s (applied potential was +1.2 V). **(B)** Expanded view of amperometric i-t curve in Fig. **A**.

The linear range was found as 100 µM - 1 mM with the detection limit of 15.62 µM (Fig. S11). However, no voltammetric response was observed in the absence of nitrite ions. In the amperometric i-t curve, the current response signals were monitored for successive injections of 10 µM to 100 µM nitrite ions at a regular time interval of 60 s in a homogeneously stirred solution of 0.1 M PBS (Fig. 9).

The well identified signals were obtained for every addition of nitrite and the detection limit was calculated as 3.98 µM (Fig. S12). The sensing performance of the $ZnTiO_3$-TiO_2 composite film was compared with other previously reported sensor materials for the detection of nitrite ions and the results are summarized in Table 3 which indicates that the detection limit of the present sensor is comparable to the other oxide materials. The LOD value calculated from amperometric i-t curve was below the guidance level of 65 µM for short–term exposure and the provisional guidance level of 4.3 µM for long–term exposure for nitrite ions according to the World Health Organization.[48]

Table 3. Comparison of performance of various electrochemical sensors for nitrite (NO_2^-) detection.

Sensor material	Analytical technique	Limit of detection (LOD)	Ref.
MnO_2/QPOE	Amperometry	0.36 µM	49
Au@Fe_3O_4/Cys	Differential Pulse Voltammetry	0.82 µM	50
Flower like-CuO	Amperometry	0.36 µM	51
CuO-Graphite	Cyclic voltammetry	0.6 µM	52
MnO_2 nanorods	Amperometry	0.29 µM	53
$ZnTiO_3$-TiO_2 microshperes	Amperometry	3.98 µM	Present work

The selectivity of the $ZnTiO_3$-TiO_2 composite oxides film for the determination of nitrite was investigated by adding various possible interferents and observing the change in current (Fig. 10). The amperometric i–t curve was continuously recorded for the successive additions of nitrite and interferents in a homogeneously stirred 0.1 M PBS (pH 7.2). After a few additions of 100 µM of nitrite, the response signal was monitored by the addition of common interferents such as Na_2CO_3, NaF, NH_4Cl, $CaCl_2$, $NaNO_3$ and $MgSO_4$ (Fig. 10). It is clearly displayed that the current signal increased only when the nitrite ion was added. After three successive additions of 100 µM nitrite ions, 1000 µM of each common interferent was added one by one separately at a regular interval of 60 s to the same solution. While the addition of interferents did not show any current response, the addition of 100 µM of nitrite to the same stirred solution resulted in a quick response with almost the same magnitude in current. The similar process was repeated one more time with common interferents and no change in current response was observed. These results demonstrate that the detection of nitrite even in the presence of 10 fold excess of common interferents is possible and the $ZnTiO_3$-TiO_2 composite film possesses high selectivity toward nitrite ions over other common interferents.

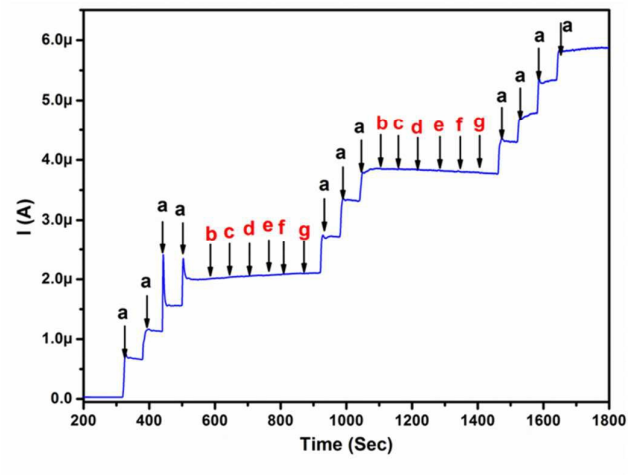

Fig. 10. Amperometric i–t curve of $ZnTiO_3$-TiO_2 composite thin film for the addition of 100 µM nitrite (**a**) and each 1000 µM addition of other interferences such as Na_2CO_3 (**b**), NaF (**c**), NH_4Cl (**d**), $CaCl_2$ (**e**), $NaNO_3$ (**f**) and $MgSO_4$ (g) in 0.1 M PBS (pH 7.2) at a regular time interval of 60 sec (applied potential was +1.2 V).

4. Conclusions

In summary, the heterobimetallic precursor $[Zn_2Ti_4(\mu\text{-}O)_6(TFA)_8(THF)_6]\cdot THF$ (**1**), designed and synthesised by reacting zinc (II) acetate with titanium (IV) isopropoxide in a molar ratio of 1:2 in the presence of trifluoroacetic acid in tetrahydofuran, was characterized by physical and spectroscopic techniques. The pyrolysis pattern of the precursor indicates its facile thermal decomposition at the relatively low temperature of 500 ˚C. The high solubility of precursor (**1**) in various organic solvents such as methanol, THF and acetonitrile makes it proficient for the growth of zinc titanate-titania composite thin films on FTO conducting glass substrate by aerosol assisted chemical vapour deposition method. Scanning electron microscopic images indicate that size, shape and textures of microspherical architectures of composite oxides films are greatly influenced by the type of deposition solvent used. The fabricated films have been identified as a 1:1 ratio of zinc titanate: titania $ZnTiO_3$:TiO_2 phases by X-ray diffraction and Raman spectroscopy with compositional analysis revealing zinc to titanium ratios of 1: 2. The UV-visible data of the films showed the direct band gap nature of the material with E_g = 3.1 eV. The electrochemical sensing capability of $ZnTiO_3$-TiO_2 microspherical composite film electrode towards nitrite ions was measured by linear scanning volatmmetry and amperometric curve techniques and the detection limits were found to be 15.62 and 3.98 µm respectively. The newly investigated electrochemical sensor also displayed selectivity towards nitrite ions in the presence of other common interferents.

Acknowledgements

The authors acknowledge the High-Impact Research scheme grant number: UM.C/625/1/HIR/242, UMRG scheme grant number: RP007A-13AET and HIR-MOHE grant number: UM.S/P/628/3SC21 for funding.

Notes and references

1 A. Weir, P. Westerhoff, L. Fabricius, K. Hristovski and N. von Goetz, *Environ. Sci. Technol.*, 2012, **46**, 2242-2250.
2 Y. V. Kolen'ko, K. A. Kovnir, A. I. Gavrilov, A. V. Garshev, P. E. Meskin, B. R. Churagulov, M. Bouchard, C. Colbeau-Justin, O. I. Lebedev and G. Van Tendeloo, J. Phys. Chem. B, 2005, 109, 20303-20309.
3 M. Zhang, Z. Yuan, J. Song and C. Zheng, Sensors Actuat. B-Chem., 2010, 148, 87-92..
4 J. Chen, B. Li, J. Zheng, J. Zhao and Z. Zhu, J. Phys. Chem. A, 2012, 116, 14848-14856.
5 Y.-C. Nah, A. Ghicov, D. Kim, S. Berger and P. Schmuki, J. Am. Chem. Soc., 2008, 130, 16154-16155..
6 H. J. Haugen, M. Monjo, M. Rubert, A. Verket, S. P. Lyngstadaas, J. E. Ellingsen, H. J. Rønold and J. C. Wohlfahrt, Acta Biomater., 2013, 9, 5390-5399..
7 A. Mills, J. Wang and M. McGrady, J. Phys. Chem. B, 2006, 110, 18324-18331.
8 C. W. Dunnill, A. Kafizas and I. P. Parkin, Chem. Vap. Deposition, 2012, 18, 89-101.
9 D. O. Scanlon, C. W. Dunnill, J. Buckeridge, S. A. Shevlin, A. J. Logsdail, S. M. Woodley, C. R. A. Catlow, M. J. Powell, R. G. Palgrave and I. P. Parkin, Nat. Mater., 2013, 12, 798-801..
10 J. Yang, J. Akbarzadeh, C. Maurer, H. Peterlik and U. Schubert, J. Mater. Chem., 2012, 22, 24034-24041.
11 Y.-H. Yu and M. Xia, Mater. Lett., 2012, 77, 10-12..
12 Y.-C. Liang, C.-Y. Hu and Y.-C. Liang, CrystEngComm, 2012, 14, 5579-5584..
13 Y.-S. Chang, Y.-H. Chang, I.-G. Chen, G.-J. Chen, Y.-L. Chai, T.-H. Fang and S. Wu, Ceram. Int., 2004, 30, 2183-2189.
14 L. G. Teoh, W.-H. Lu, T. H. Lin and Y.-C. Lee, J. Nanomater., 2012, 2012, 20.

15 L. Borgese, E. Bontempi, L. E. Depero, P. Colombi and I. Alessandri, CrystEngComm, 2011, 13, 6621-6624.
16 G. Krylova, A. Brioude, S. Ababou-Girard, J. Mrazek and L. Spanhel, Phys. Chem. Chem. Phys., 2010, 12, 15101-15110.
17 S. Ke, X. Cheng, Q. Wang, Y. Wang and Z. Pan, Ceram. Int., 2014, 40, 8891-8895.
18 Y. Deng, Q. Lv, S. Wu and S. Zhan, Dalton Trans., 2010, 39, 2497-2503..
19 A. Nikitinskii, L. Bochkarev, R. Voronin, S. Y. Khorshev, Y. A. Kurskii and M. Bochkarev, Russ. J. Gen. Chem., 2004, 74, 1194-1196..
20 C. Artner, A. Koyun, M. Czakler and U. Schubert, Eur. J. Inorg. Chem., 2014, 5008-5014.
21 M. A. Mansoor, M. Mazhar, V. McKee and Z. Arifin, Polyhedron, 2014, 75, 135-140.
22 M. A. Ehsan, A. A. Tahir, M. Hamid, M. Mazhar, K. Wijayantha and M. Zeller, Inorg. Chim. Acta , 2011, 376, 189-194.
23 M. A. Ehsan, M. A. Mansoor, M. Mazhar, A. A. Tahir, M. Hamid and K. Upul Wijayantha, Appl. Organomet. Chem., 2012, 26, 493..
24 A. A. Tahir, M. Mazhar, M. Hamid, K. U. Wijayantha and K. C. Molloy, Dalton Trans., 2009, 3674-3680..
25 A. A. Tahir, M. Hamid, M. Mazhar, M. Zeller, A. D. Hunter, M. Nadeem and M. J. Akhtar, Dalton Trans., 2008, 1224-1232..
26 M. Hamid, A. A. Tahir, M. Mazhar, M. Zeller and A. D. Hunter, Inorg. Chem., 2007, 46, 4120-4127.
27 S. A. Bakar, S. T. Hussain and M. Mazhar, New J. Chem., 2012, 36, 1844-1851..
28 M. A. Mansoor, A. Ismail, R. Yahya, Z. Arifin, E. R. Tiekink, N. S. Weng, M. Mazhar and A. R. Esmaeili, Inorg. Chem., 2013, 52, 5624-5626..
29 C. S. Bruning-Fann and J. Kaneene, Vet. Hum. Toxicol., 1993, 35, 521-538..
30 Bruker APEX2 and SAINT, Bruker AXS Inc., Madison, WI, USA, 2007..
31 Sheldrick, G. M. Acta Crystallogr., Sect. A: Found. Crystallogr., 2008, 64, 112..
32 L. J. Barbour, J. Supramol. Chem., 2001, 1, 189-191.
33 D. V. K. Wieghardt, Y. H. Tsai, C. Kruger Inorg. Chim. Acta 1985, 99, L25..
34 A. A. Tahir, H. A. Burch, K. Wijayantha and B. G. Pollet, Int. J. Hydrogen Energy, 2013, 38, 4315-4323.
35 M. A. Ehsan, H. N. Ming, M. Misran, Z. Arifin, E. R. Tiekink, A. P. Safwan, M. Ebadi, W. J. Basirun and M. Mazhar, Chem. Vap. Deposition, 2012, 18, 191-200..
36 S. F. BARTRAM and R. A. SLEPETYS, J. Am. Ceram. Soc., 1961, 44, 493-499..
37 N. M. M. Kato, N. Ishizawa and H. Seki, Golden Book of Phase Transitions, Wroclaw, 2002, 1, 1 - 123.
38 E. P. Meagher, C. F. Schwerdtfeger and M. Horn, Golden Book of Phase Transitions, Wroclaw, 2002, 1, 1 - 123..
39 X. Liu, Z. Jin, S. Bu, T. Yin, J. Sol-Gel Sci. Technol. 2005, 36, 103.
40 C. Edusi, G. Sankar, and I. P. Parkin Chem. Vap. Deposition 2012, 18, 126–132.
41 M. Sugiura and K. Ikeda, J. Ceram. Soc. Jpn., 1947, 55, 62.
42 Y.-C. Lee, Y.-L. Huang, W.-H. Lee and F.-S. Shieu, Thin Solid Films, 2010, 518, 7366-7371..
43 M. Nikolić, N. Obradović, K. Paraskevopoulos, T. Zorba, S. Savić and M. Ristić, J. Mater. Sci., 2008, 43, 5564-5568..
44 Y.-S. Chang, Y.-H. Chang, I.-G. Chen, G.-J. Chen and Y.-L. Chai, J. Cryst. Growth, 2002, 243, 319-326.
45 N. T. Nolan, M. K. Seery and S. C. Pillai, Chem. Mater., 2011, 23, 1496-1504..
46 A. Pandikumar, N. Yusoff, N. M. Huang and H. N. Lim, Microchim. Acta, 2014, 1-10..
47 P. Rameshkumar, P. Viswanathan and R. Ramaraj, Sensors Actuat. B- Chem., 2014, 202, 1070-1077.
48 M. Khairy, R. O. Kadara and C. E. Banks, Anal. Methods, 2010, 2, 851-854.
49 C. Xia, W. Ning and G. Lin, *Sensors Actuat. B- Chem.*, 2009, **137**, 710-714.
50 C. Yu, J. Guo and H. Gu, Electroanal., 2010, 22, 1005-1011.
51 L. Zhang, F. Yuan, X. Zhang and L. Yang, Chem. Central J., 2011, 5, 75-83.
52 B. Šljukić, C. E. Banks, A. Crossley and R. G. Compton, Electroanal., 2007, 19, 79-84.
53 J.-J. Feng, P.-P. Zhang, A.-J. Wang, Y. Zhang, W.-J. Dong and J.-R. Chen, J. Colloid Interface Sci., 2011, 359, 1-8.